

Geophysical Research Letters



RESEARCH LETTER

10.1029/2020GL091839

Key Points:

- Oceanic thermal feedback acts on the marine atmospheric boundary layer dynamics at daily time-scale
- The downward momentum mixing mechanism imprints cloud cover and rain
- SST gradients partially drive cloud structures and rainfall over the Mediterranean Sea

Supporting Information:

Supporting Information may be found in the online version of this article.

Correspondence to:

F. Desbiolles,
fabien.desbiolles@unimib.it

Citation:

Desbiolles, F., Alberti, M., Hamouda, M. E., Meroni, A. N., & Pasquero, C. (2021). Links between sea surface temperature structures, clouds and rainfall: Study case of the Mediterranean Sea. *Geophysical Research Letters*, 48, e2020GL091839. <https://doi.org/10.1029/2020GL091839>





Received 24 NOV 2020

Accepted 15 APR 2021

© 2021. The Authors.

This is an open access article under the terms of the [Creative Commons Attribution-NonCommercial-NoDerivs License](https://creativecommons.org/licenses/by-nc-nd/4.0/), which permits use and distribution in any medium, provided the original work is properly cited, the use is non-commercial and no modifications or adaptations are made.

Links Between Sea Surface Temperature Structures, Clouds and Rainfall: Study Case of the Mediterranean Sea

Fabien Desbiolles^{1,2} , Maria Alberti¹, Mostafa E. Hamouda^{1,3} , Agostino N. Meroni^{1,4,5} , and Claudia Pasquero^{1,6} 

¹Department of Earth and Environmental Sciences, Università di Milano - Bicocca, Milan, Italy, ²Istituto Nazionale di Oceanografia e di Geofisica Sperimentale – OGS, Trieste, Italy, ³Astronomy and Meteorology Department, Faculty of Science, Cairo University, Cairo, Egypt, ⁴Department of Civil and Environmental Engineering, Politecnico di Milano, Milan, Italy, ⁵CIMA Research Foundation, Savona, Italy, ⁶Istituto di Scienze dell'Atmosfera e del Clima, Consiglio Nazionale delle Ricerche, Turin, Italy

Abstract Using 25 years of ERA5 reanalysis data, this study shows that wind divergence is partially driven by small-scale sea surface temperature (SST) patterns via their effect on the boundary layer stability. Moreover, strong warm-to-cold fronts (the upper quartile) are associated with a mean increase of cloud cover of $10\% \pm 5\%$ and a mean increase in the probability of a rain event of $15\% \pm 6\%$, with respect to the average values. The cloud and rainfall dependence on SST fronts is more pronounced in Fall, probably due to the stronger SST gradients present at the end of the summer season.

Plain Language Summary Oceanic thermal structures impact surface winds, low-level clouds, and rainfall. Using reanalysis data over the Mediterranean Sea, this paper shows that the reduced stability over warm patches increases the coupling of surface winds with winds aloft. This process affects the entire marine atmospheric boundary layer. This results in a cloud cover and rainfall response: when the wind blows from warm to cold (from cold to warm) water, a converging (diverging) cell is enhanced, increasing (decreasing) low-cloud cover and favoring by about 15% a rain event.

1. Introduction

Ocean and atmosphere communicate through exchanges at the air-sea interface, a complex surface in perennial disequilibrium. At large scales, atmospheric dynamics force ocean variability (Gill, 2016) as strong winds enhance surface turbulent heat fluxes and generate upper ocean mixing, reducing sea surface temperature (SST). At finer scales, $\mathcal{O}(100\text{km})$, ocean structures influence the atmospheric dynamics (Chelton et al., 2001), impacting air temperature, frictional stress, and the marine atmospheric boundary layer (MABL) stability. The upper ocean and lower atmosphere layers interact through different processes forming a feedback loop (e.g., Strobach et al. (2020)).

Ocean thermal structures affect the stability of the air-column and its thermodynamical properties through thermal and dynamical adjustments of the MABL (Small et al., 2008). The resulting small-scale processes, called thermal feedback, have important upscale and remote impacts at seasonal timescales on local surface wind (Chelton et al., 2004), basin-scale atmospheric circulation (Desbiolles et al., 2018), cloud cover, rainfall location over ocean - as shown in long-term average over the Gulf Stream (Minobe et al., 2008) or in composite analyses over Southern Ocean eddies (Frenger et al., 2013) - and climatic variability of heat/tropical lows inland (Desbiolles et al., 2020). Thus, small-scale air-sea interactions significantly affect the water cycle.

Two main mechanisms have been proposed to describe the surface wind response to small-scale variability of SST: the downward momentum mixing (hereafter DM), notably introduced by Hayes et al. (1989), and the pressure adjustment (PA), highlighted by Lindzen and Nigam (1987). The DM mechanism brings into play large eddies within the MABL, stimulated by turbulent fluctuations of momentum, temperature and moisture, that redistribute horizontal momentum in the vertical direction (Small et al., 2008). This process modifies the MABL stability over SST patterns (Businger & Shaw, 1984), entailing, as a net effect, weaker (stronger) surface winds over the cold (warm) flank of an SST gradient (Wallace et al., 1989). As a consequence, a positive correlation emerges between wind divergence and downwind SST gradient (e.g., Chelton

et al., 2004, 2007; Desbiolles et al., 2014; Meroni, Parodi, & Pasquero, 2018; O'Neill et al., 2003; 2005). The PA mechanism causes surface wind divergence due to surface pressure anomalies forced by atmospheric temperature patterns, driven themselves by the SST spatial variability (Lindzen & Nigam, 1987). It results in a linear relationship between surface wind divergence and SST Laplacian (Foussard et al., 2019; Small et al., 2008).

Thus, DM and PA mechanisms affect near-surface winds and then turbulent properties at mesoscales (Small et al., 2008). Recent studies show concomitant observations of anomalies in wind speed and clouds over mesoscale energetic western boundary currents; such as Gulf Stream (Minobe et al., 2008; Park et al., 2006), Kuroshio extended region (Xu et al., 2011) and Aghulas retroflexion area (O'Neill et al., 2005). Also the link with the change of rain rate has been documented over large and permanent Western boundary fronts (e.g., Xu et al., 2011; Minobe et al., (2008) for the Kuroshio and Gulf Stream, respectively). More precisely, Minobe et al., (2008) showed that under the PA mechanism, on annual timescale, rainbands develop over the warm side of the front. Moreover, cloud and rain responses have been highlighted not only over large and permanent structures, but also over shorter timescale transient anomalies, such as the cold wakes of tropical storms (Ma et al., 2020), over which PA dominates (Pasquero et al., 2021), and in correspondence of eddies of different size, with the prevailing of the DM mechanism (Liu et al., 2018; Park et al., 2006; Perlin et al., 2020; Rouault et al., 2016; Villas Boas et al., 2015; Wang et al., 2019). For example, Frenger et al., (2013) reported the composite response of the near-surface wind dynamics, clouds and rainfall over warm and cold eddies in the Southern ocean and concluded that transient ocean structures significantly alter atmospheric weather regimes.

In this study, we focus on the mid-latitude Mediterranean Sea, a semi-enclosed basin, which is subject to numerous local and regional atmospheric processes. In particular, air-sea interactions and the complex orography surrounding the basin favor the development of heavy precipitation events, such as those associated with mesoscale convective systems (Fiori et al., 2017; Nuissier et al., 2008), that generally develop over the sea and are responsible for a significant fraction of the annual rainfall in coastal regions (Ducrocq et al., 2008; Fiori et al., 2014). The mean SST has been shown to control the rainfall amount of those events by modifying the atmospheric stability: the warmer the sea, the more unstable the air-column and the higher the rainfall volume (Lebeaupin et al., 2006; Meroni, Renault, et al., 2018; Pastor et al., 2001). Fine-scale SST structures and gradients, on the other hand, generate a differential heating into the atmosphere and modify the surface wind (Cassola et al., 2016; Meroni, Parodi, & Pasquero, 2018; Senatore et al., 2020). Meroni et al., (2020) have shown that the DM mechanism drives the near-surface wind response over the Mediterranean, especially during Fall.

Following Meroni et al., (2020), this paper aims to describe the daily timescale response of the MABL to SST patterns over the Mediterranean, exploiting the relatively high-resolution ERA5 reanalysis (Hersbach et al., 2020). To complement Meroni et al., (2020), which used 10 m neutral-equivalent wind and SST based on satellite retrievals, we exploit here the ERA5 reanalysis product and focus on the vertical structure of the atmospheric response and the potential impact on cloud cover and rainfall.

2. Data and Metrics Used

This study uses ERA5 (Hersbach et al., 2020) which is the reanalysis data set with the finest spatial resolution available (roughly 30 km globally), obtained with a 4DVAR data assimilation approach with the integrated forecast system. More specifically, we use SST, horizontal wind, cloud cover fraction from 1000 to 700 hPa every 25 hPa, and total and convective rain, all at daily frequency taken at midnight UTC. The statistical analysis are performed in the period 1990–2014. It is worth remarking that, despite the nominal resolution of about 30 km, ERA5 acknowledges an effective resolution of about 100 km.

In order to better assess SST effects on wind divergence, a coastal mask is applied on each field. It covers a strip of about 50 km off the coast over which atmospheric dynamics is also driven by several different processes such as land-sea breeze and orographic effects (e.g., Drobinski et al., 2018; Buzzi et al., 2020). A discussion about the width of the coastal mask is provided in the supportive information document.

Correlations between wind convergence and SST derivative fields are computed. The DM mechanism results in a correlation between wind divergence, $\nabla \cdot \mathbf{u}$, and downwind SST gradient, $\nabla SST \cdot \hat{k}$, where \hat{k} is the unit vector aligned with the wind direction. The sign of the downwind SST gradient is determined by the relative direction of the 10 m instantaneous wind and the SST gradient: negative (positive) when the wind blows from warm-to-cold (cold-to-warm) water. The PA mechanism results in a positive correlation between $\nabla \cdot \mathbf{u}$ and SST Laplacian, $\nabla^2 SST$. The two correlation coefficients, stressing an active DM and/or PA mechanisms, are calculated both temporally and spatially.

The significance of the correlation coefficients is determined by the calculation of the 95% confidence interval of the null hypothesis of zero correlation, using the effective number of degrees of freedom following Press et al., (1992); Bretherton et al., (1999). For details, the reader is referred to appendix A of Meroni et al., (2018). It is worth noting that all the confidence intervals are wider than in Meroni et al., (2020) due to the slightly coarser effective resolution of ERA5 compared to satellite observations.

Section 4 shows the effect of air-sea interactions on low-level cloud cover and rainfall. Cloud cover fraction is integrated from 1000 to 925 hPa. The uppermost pressure level used for the cloud cover analysis roughly corresponds to the MABL top (see supporting information). Its choice is based on the vertical structure of MABL response to SST gradients highlighted in Figure 2. The total and convective rain fields are analyzed regardless of the amount of rain: each pixel with a strict positive rainfall has been flagged as a rain event.

Details about methodology are given to complement the following results in the supporting information.

3. MABL Dynamics Responses to SST Patterns

3.1. Surface Responses

Figure 1 shows the temporal (upper) and spatial (bottom panels) correlation coefficients between $\nabla \cdot \mathbf{u}$ and $\nabla SST \cdot \hat{k}$ (left panels) and between $\nabla \cdot \mathbf{u}$ and $\nabla^2 SST$ (right panels). The spatial correlations are shown in Figures 1c and 1d as a climatology.

It emerges that, at daily timescale, DM is prevailing over PA in shaping the 10 m wind divergence. Indeed, wind divergence is positively correlated with downwind SST gradient while it is mostly non-significantly correlated with SST Laplacian (Figures 1a and 1b). Therefore, the DM mechanism acts almost everywhere over the Mediterranean basin, except in some locations where the wind dynamics is driven by other processes. This is the case for the Adriatic and Alboran basins, which are narrow seas where wind dynamics is constrained by the surrounding land. Temporal correlation between wind divergence and downwind SST gradient can be important (i.e., coefficients greater than 0.5 in the Gulf of Lions and North of the border between Libya and Egypt).

The seasonal mean of the spatial correlation also shows that wind divergence is significantly related to downwind SST gradient and not to SST Laplacian (Figures 1c and 1d). During Fall, correlations are higher (Figure 1c), which can be explained by the presence of stronger SST gradients (see supporting information). This transitional season is the period during which storms and atmospheric depressions develop over a thermally stratified ocean. Resulting SST gradients are then intense and act back on surface winds.

Meroni et al., (2020) found that during Fall, the probability of having strong wind convergence over warm-to-cold SST fronts is twice as high as the probability of having it over cold-to-warm fronts. Together with the positive and significant correlations introduced above, this is in agreement with the action of the DM mechanism, suggesting that the presence of warm-to-cold fronts affects the overlying atmosphere. In particular, this behavior is observed for strong convergence values, typically associated with atmospheric fronts (see supporting information).

3.2. Vertical Structure

Figure 2 shows boxplot of the spatial correlation between $\nabla \cdot \mathbf{u}$ from the surface to 700 hPa and $\nabla SST \cdot \hat{k}$ for the entire period and Fall only. Note that the downwind SST gradient is taken with respect to the 10 m wind direction, regardless of the wind direction at higher levels. The shaded area along the 0 correlation

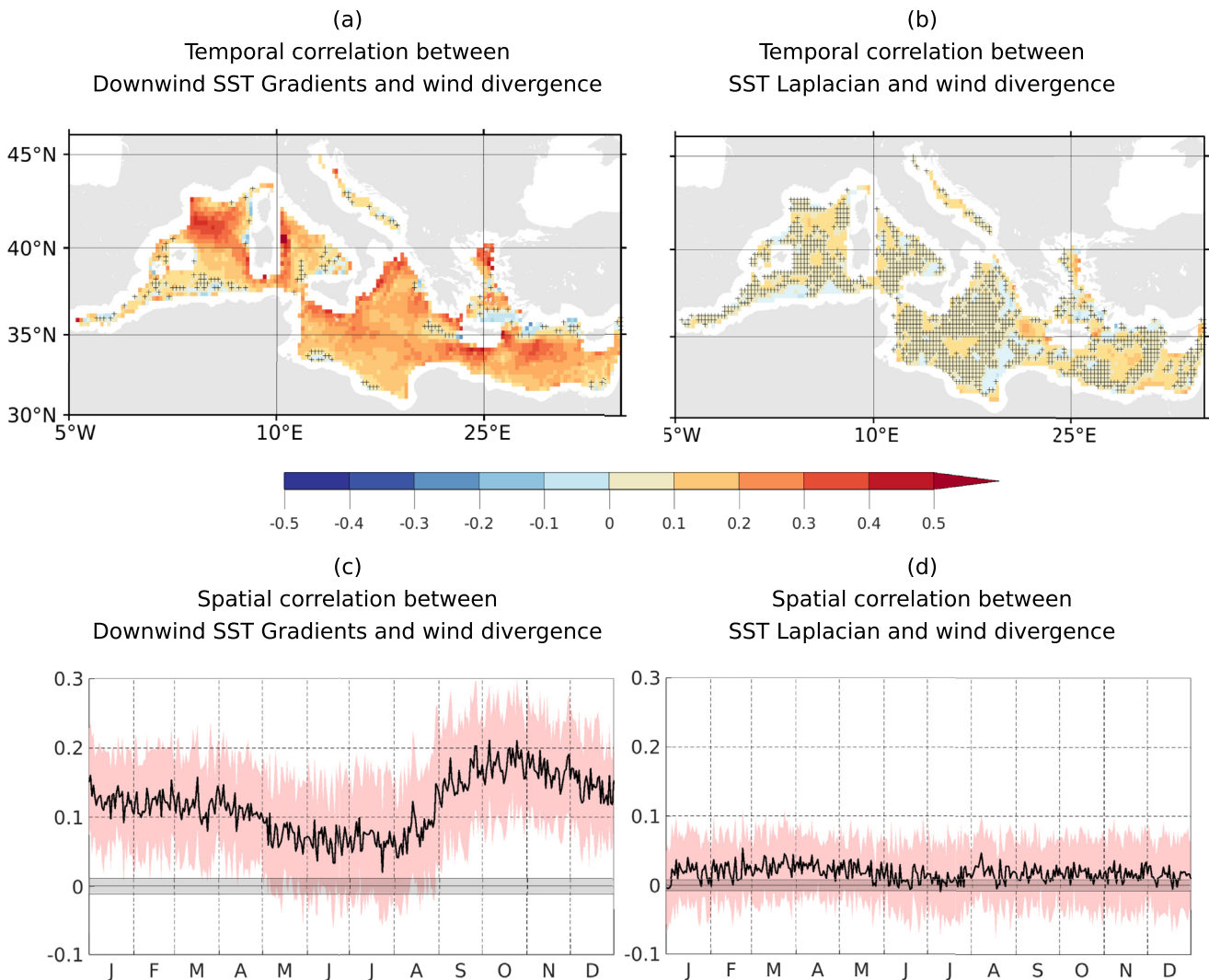


Figure 1. (a and b) Temporal correlation between $\nabla \cdot \mathbf{u}$ and (a) $\nabla S T \cdot \hat{k}$ and (b) $\nabla^2 S T$ at the daily time scale. Black “+” marks denote pixels where correlations are non-significant (see text for details). (c and d) Seasonal cycle of spatial correlation between $\nabla \cdot \mathbf{u}$ and (c) $\nabla S T \cdot \hat{k}$ and (d) $\nabla^2 S T$. The solid line represents the mean and the red shaded area the standard deviation around that mean. The black shaded area corresponds to the 95% confidence interval.

represents the 95% confidence interval. On the first y-coordinate the statistics are calculated with the neutral stability hypothesis (\mathbf{u}_{10}^N) on both fields.

Mean spatial correlations between wind divergence and downwind SST gradient are significant from the surface (i.e., 10 m) up to 925 hPa for the entire period and Fall only (Figures 2a and 2b, respectively). Despite during Fall correlations admit higher values (Figure 2b), the vertical structure remains the same. The coefficients decrease with altitude but remain relatively important up to 925 hPa. In both analyzed periods, the time mean spatial correlation crosses the zero line at 875 hPa, but is non-significant from 925 hPa and above. Therefore, we conclude that the imprint of SST gradients is not only present at the surface but is significantly visible up to 925 hPa, encompassing the entire MABL at least 80% of the time (see supporting information). Indeed, the DM mechanism affects fluctuations of momentum over the MABL thickness since it enhances mixing of momentum from the top of the MABL to the surface (Spall, 2007; Wallace et al., 1989).

It is worth noting here that neutral-equivalent winds have been shown to be stronger (weaker) than actual winds in unstable (stable) boundary layers (O’Neill et al., 2012). This implies that higher correlation coefficients are expected when using neutral-equivalent winds with respect to the actual ones, as also discussed

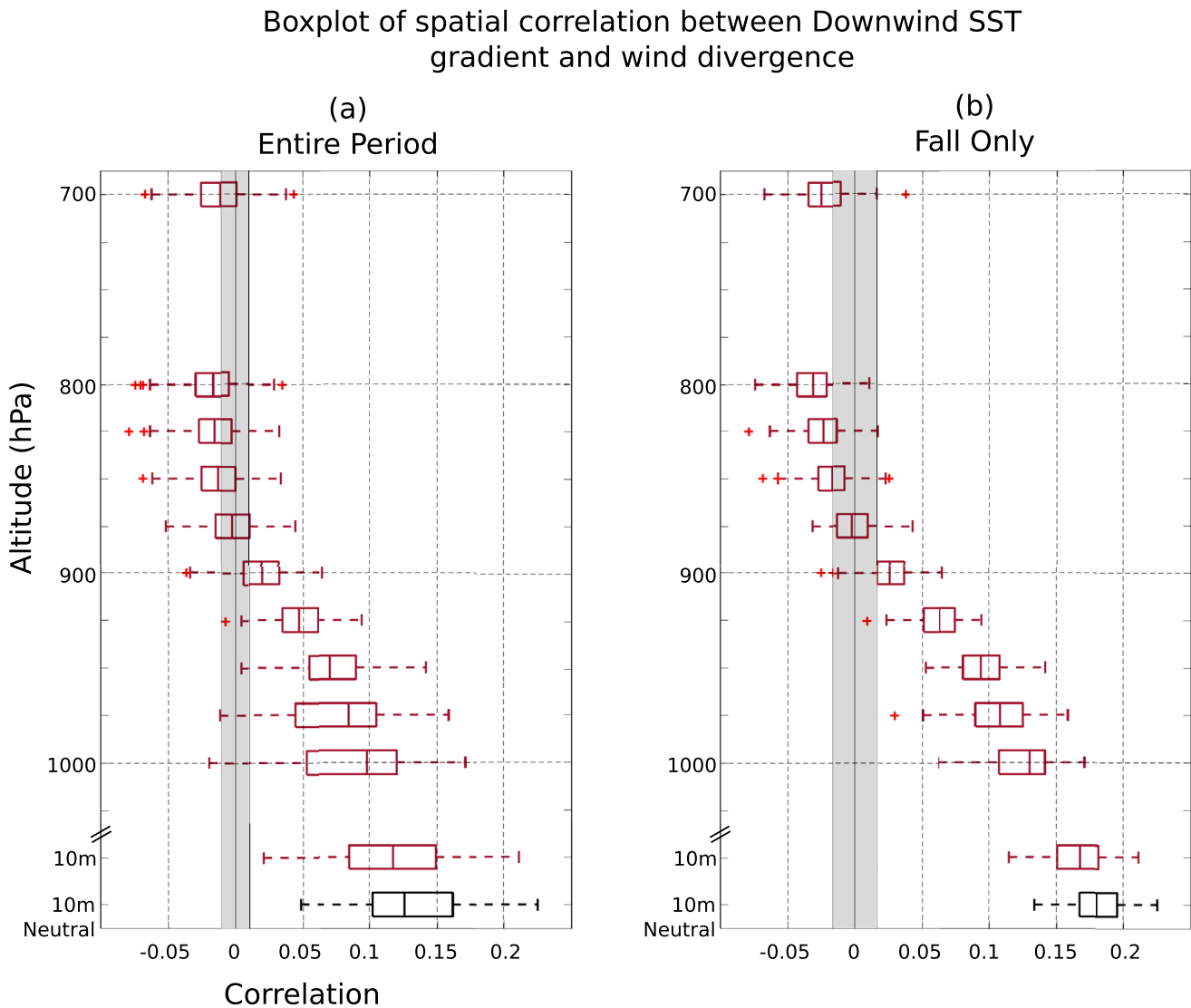


Figure 2. Boxplot of the spatial correlation between $\nabla \cdot \mathbf{u}$ at different vertical levels and $\nabla \text{SST} \cdot \hat{k}$ for (a) the entire period and (b) Fall only. The vertical shaded area represents the 95% confidence interval. The black boxplot (shown on the lowest level) represents the statistics using 10 m neutral-equivalent winds.

in Meroni et al. (2020). This is the case here (Figure 2) but the difference in the mean correlation ($\sim 1\%$) is non-significant. This confirms that the use of satellite-derived neutral-equivalent wind fields does not impact the overall correlation between the two fields, even if the coupling coefficient differs (e.g., Renault et al. (2019)).

4. Effect on Cloud Cover and Rainfall

Figure 3 shows the relative change of cloud fraction (in %) as a function of wind divergence (upper) and downwind SST gradient (bottom panels) for the entire period and Fall only. Figure 4 is built in the same way but displays the relative change of total and convective rainfall events. In all panels, the response in cloud cover and rain is analyzed statistically every 5% bins of the distribution of the considered field (either $\nabla \cdot \mathbf{u}$ or $\nabla \text{SST} \cdot \hat{k}$). The gray shaded area around the 0 line represents the 95% range of expected values of the relative change in the null hypothesis (cloud cover and total rain events independent of the considered fields). As convective rain admits a large confidence interval ($\sim 30\%$), the relative change in convective rain events is only shown when it is greater than this reference level. Notably, this never happens in panels c and

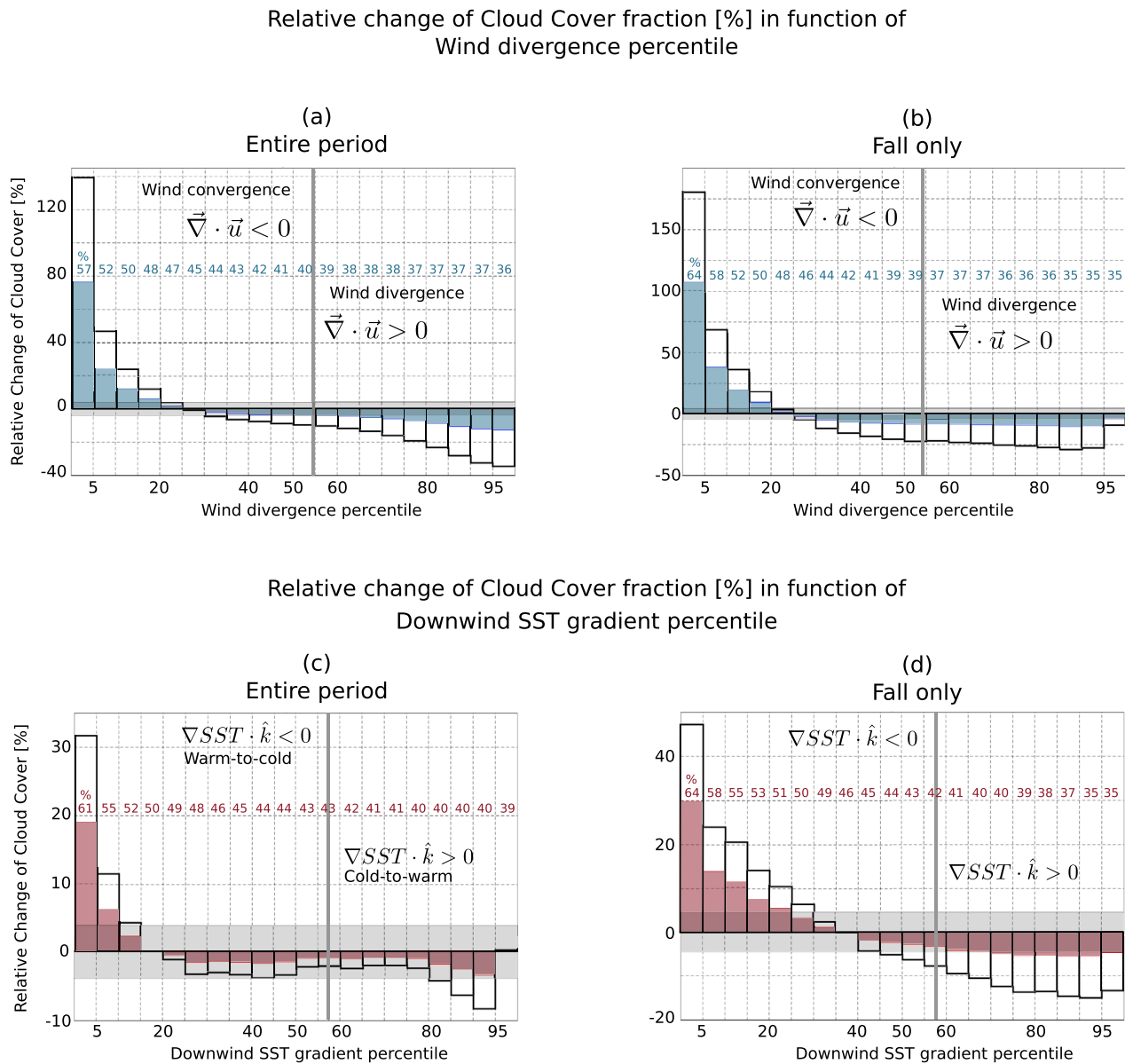


Figure 3. Percentage of cloud fraction change as a function of $\nabla \cdot \mathbf{u}$ (a and b) and $\nabla SST \cdot \hat{k}$ (c and d) for the entire period and Fall only. Cloud cover fraction is integrated from 1000 to 925 hPa. The vertical gray solid line represents the percentile of the distribution from which the metric considered changes sign. Each x-bin represents 5% of the distribution during the period of analysis. The gray shaded area represents the reference value of mean change $\pm 1.96\sigma_0$ of 5% of randomly sampled integrated cloud cover fraction calculated 1000 times. On panels a and b (c and d), the blue (red) areas and numbers indicate the fraction of events in each bin associated with $\nabla SST \cdot \hat{k} < 0$ ($\nabla \cdot \mathbf{u} < 0$).

d, as discussed below. In Figures 3a and 3b, blue histograms and numbers show the percentage of negative $\nabla SST \cdot \hat{k}$ events (warm-to-cold fronts) in each class of $\nabla \cdot \mathbf{u}$. The red color on Figures 3c and 3d, represents the percentage of wind convergence events in each class of $\nabla SST \cdot \hat{k}$.

Cloud cover has a clear response for extreme convergence events, with an increase of about 140% and 175%, for the entire period and Fall only, respectively (Figures 3a and 3b). This means that the cloud fraction more than doubles in case of extreme convergence. Over those events, 57% of them correspond to a negative downwind SST gradient. During Fall, this percentage is higher (almost 66%, i.e., 2/3) and indicates that the probability of having surface convergence over a warm-to-cold front is twice as large as the opposite one, in

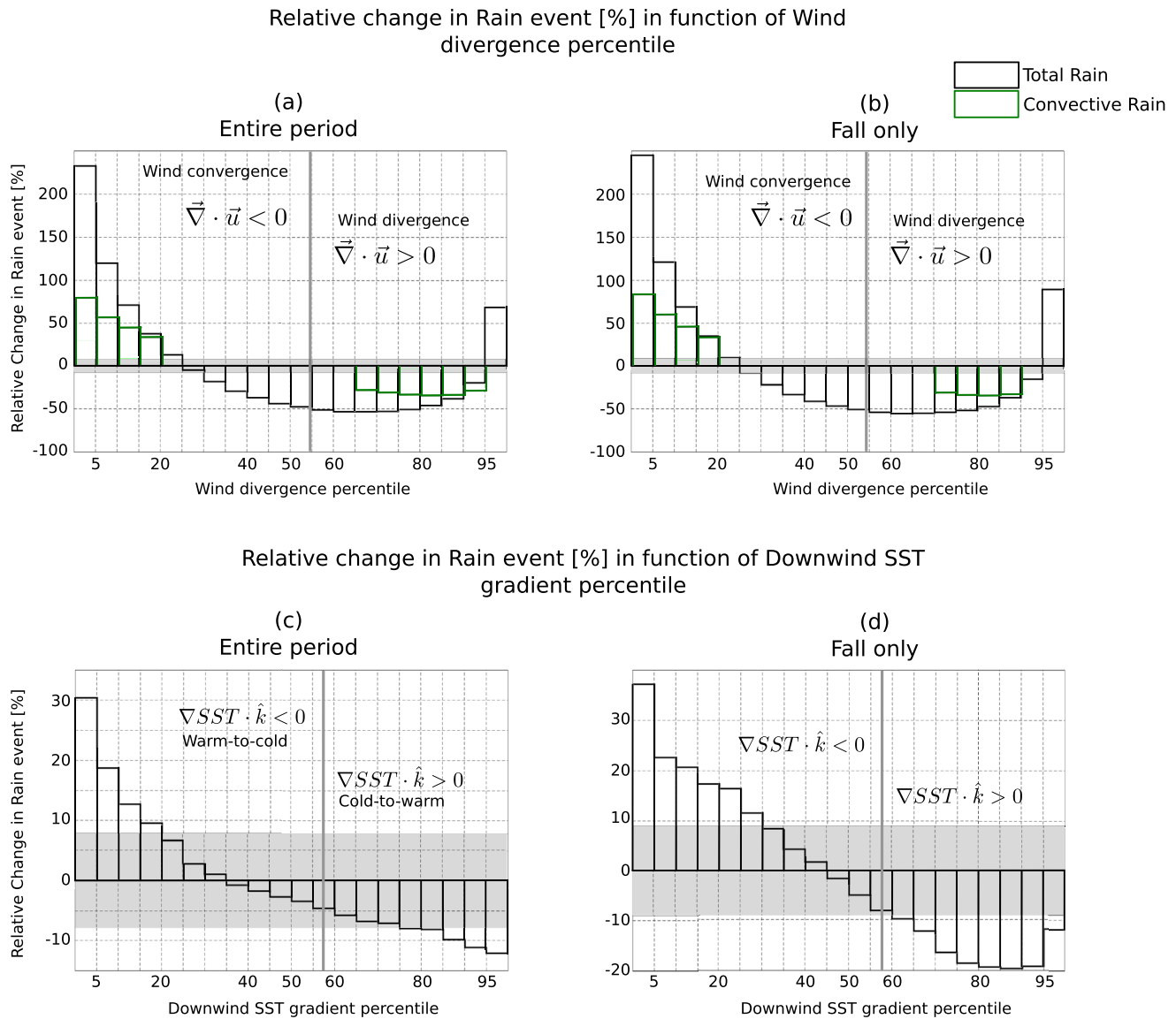


Figure 4. Relative change of total (black) and convective (green) rain events as a function of $\nabla \cdot \mathbf{u}$ (upper panels) and $\nabla SST \cdot \hat{k}$ (bottom panels) for the entire period (left panels) and Fall only (right panels). The vertical gray solid line represents the percentile of the distribution from which the surface metric considered changes sign. Each x -bin represents 5% of the distribution. The gray shaded area around 0 represents the reference value of mean change $\pm 1.96\sigma_0$ of 5% of randomly sampled total rain events calculated 1,000 times. Only significant changes of convective rain events are shown.

agreement with the findings of Meroni et al., (2020). The relative change of cloud fraction monotonically decreases for increasing wind divergence.

For strong wind divergence cases, cloud cover decreases by about 40% for the entire period and by far less during Fall (Figures 3a and 3b); the latter result will be discussed later, when rain events will be presented. Over all wind divergence events, about 2/3 correspond to a positive $\nabla SST \cdot \hat{k}$. This confirms that it is predominantly more likely to have wind divergence over a positive downwind SST gradient, as per the DM mechanism. In fact, low-level cloud cover fraction has significant changes in association to underlying SST patterns, as shown in Figures 3c and 3d, irrespective of the upper layer thermodynamical state. During Fall, when the signal is stronger, the cloud cover fraction in the lower 5% values of $SST \cdot \hat{k}$ is about 48% higher than on average, and it is about 13% lower than on average in the upper 5% values of $SST \cdot \hat{k}$. This results in a cloud cover about 1.7 times larger in the lower 5% negative downwind SST gradient than in the upper 5% positive one.

Low-level cloud cover responds to $\nabla SST \cdot \hat{k}$ with, notably, an important increase of 30% and 45% over extreme negative values for the entire period and Fall only, respectively (Figures 3c and 3d). Therefore, an extreme negative $\nabla SST \cdot \hat{k}$, corresponding to a warm-to-cold scenario, favors wind convergence (found in $\sim 60\%$ of the cases) and cloud formation. For the entire period the signal is however not significant for the rest of the distribution (Figure 3c) but the cloud response is straightforward for the whole distribution of $\nabla SST \cdot \hat{k}$ during Fall (except from the percentile 30 to 50% for which the relative change is non-significant, Figure 3d). A large positive $\nabla SST \cdot \hat{k}$ is associated with wind divergence in $\sim 60\%$ of the cases, and with a reduction of $\sim 15\%$ of cloud cover.

Rainfall events are clearly favored by strong wind convergence, with an increase of chance of having rain of about 200% and 250% for the entire period and for Fall only, respectively (Figures 4a and 4b). The occurrence of convective rain events is also significantly larger for the strongest 20% wind convergence events. The probability of having rain events decreases with increasing $\nabla \cdot \mathbf{u}$ until it reaches a minimum at about 2/3 of the wind divergence distribution. For weak convergence and weak-to-moderate divergence winds, rainfall is suppressed compared to the average value. Remarkably, strong divergence is associated with a significant increase of the probability of having precipitation, possibly because rainfall can produce cold mesoscale downdrafts when raindrops evaporate during their fall, generating strong divergence when the downdrafts get to the surface. In other words, strong wind divergence is probably caused by precipitations, while large scale dynamics typical of the extratropical storms seldom generate strong surface wind divergence. The rain events that generate downdrafts are more likely to happen during the Fall season, as they are associated with mesoscale convective systems, whose dynamics is favored by warm SSTs. This is consistent with the small change of cloud cover associated with the strong divergence shown in Figure 3b: whereas strong divergence in surface winds suppresses low-level clouds, thick convective clouds typical of the Fall season in some cases produce strong surface wind divergence. Overall, the two processes combine to induce a negligible change in cloud cover with respect to the average conditions.

The relative change in the occurrence of rainfall events is statistically significant for large values (both positive and negative) of $\nabla SST \cdot \hat{k}$ (Figures 4c and 4d). Indeed, we find 30% and 35% more chance of having a rainfall event over strong negative downwind SST gradients during the entire period and Fall only, respectively, with respect to average conditions. For Fall (Figure 4d), the relative change in rain events remains positively significant over the lowest 30% of the distribution, and conversely, we have from 10% to 20% less rain events over the strongest positive 40% $\nabla SST \cdot \hat{k}$. No significant signal has been found for convective rainfall events.

To summarize the effects of SST patterns on cloud cover and rainfall in the Mediterranean region, we aggregated the results presented above over the upper and lower 25th percentiles of $\nabla SST \cdot \hat{k}$. The 25% strongest warm-to-cold fronts are associated with a mean increase of cloud cover of $10\% \pm 5\%$ ($25\% \pm 12\%$) and a mean increase in the probability of a rain event of $15\% \pm 6\%$ ($22\% \pm 10\%$), with respect to the average values for the entire period (Fall only). The 25% strongest cold-to-warm fronts are associated with a mean decrease of cloud cover of $4\% \pm 2\%$ ($14\% \pm 8\%$) and a mean decrease in the probability of a rain event of $10\% \pm 4\%$ ($18\% \pm 8\%$) for the entire period (Fall only).

5. Concluding Remarks

In this paper we have analyzed the links between SST patterns and wind divergence at the daily timescale over the Mediterranean Sea. Near the surface, that is, at 10 m, the wind divergence field is positively correlated with the downwind SST gradient and insignificantly correlated to the SST Laplacian (Figure 1). Thus, mesoscale air-sea interactions are controlled by the DM mechanism. This is notably the case during Fall, when correlation analysis shows larger values (Figure 1), due to stronger SST gradients found in this season. SST fronts and gradients play an important role in shaping the daily wind divergence field. Strong values of convergence are twice as likely to be found over warm-to-cold fronts. These results, shown by satellite observations in Meroni et al., (2020), are here supported by the reanalysis data.

The use of reanalysis data allowed us to verify that the DM mechanism modulates fluctuations not only at the surface but through the entire MABL thickness and that SST gradients modify wind divergence/convergence cells up to 925 hPa (see Section 3.2). As a consequence, the cloud cover in the MABL is modified

accordingly. A positive (negative) downwind SST gradient favors wind divergence (convergence) over the whole boundary layer, which leads to a significant decrease (increase) of cloud cover and rainfall events. The effects are larger when winds blow from warm-to-cold fronts than when they blow from cold-to-warm fronts, suggesting that the MABL response to a warm-to-cold front could be sharper and stronger than in the opposite case. This might indicate that the time needed to stabilize the MABL is shorter than the time needed to destabilize it, but further studies are necessary to characterize this asymmetric response. In detail, we have shown here that in correspondence of the 25% strongest positive downwind SST gradients the chances of having rainfall drop by $10\% \pm 4\%$ and conversely, in correspondence of the 25% strongest negative downwind SST gradients the chance of rainfall increase of $15\% \pm 6\%$. Overall, the chances of having rainfall in the lower quartile of the distribution of downwind SST gradient is about $27\% \pm 10\%$ larger than in upper quartile.

The use of daily data shows that SST gradients impact wind divergence over synoptic weather regimes, and not only over averaged conditions. The correlation values between downwind SST gradient and wind divergence at daily timescale are smaller, but still significant, than those obtained when fields are filtered from synoptic dynamics (as it usually done, e.g., Chelton et al., 2001; O'Neill et al., 2003). This is also the case for the statistics related to the PA mechanism, for which higher positive significant correlations are found from weekly to monthly timescales (see supporting information). It is worth noting that, from daily to monthly timescales, correlation analysis highlight that the DM is always more important than the PA mechanism in the Mediterranean. However, previous works suggest that PA mechanism might control the wind divergence response in certain conditions also at the daily and weekly scales (Li & Carbone, 2012; Ma et al., 2020).

The air-column stability, which is at the core of the DM mechanism, is not only driven by surface conditions but it also depends on the free troposphere state aloft. Together with environmental conditions (background winds, MABL height, ocean front size and intensity, etc., \enleadertwodots), which qualify and quantify the atmospheric response, remain to be deeply analyzed in order to disentangle their effects on the processes at play (e.g., Foussard et al., 2019; Kilpatrick et al., 2014; Oerder et al., 2016; Perlin et al., 2020).

Data Availability Statement

ERA5 reanalysis data set used is publicly available at <https://cds.climate.copernicus.eu/#/search?text=ERA5&type=dataset>

Acknowledgments

The authors thank the Editor Suzana Camargo and two anonymous reviewers. The study is funded by the European Space Agency, ESA-CONTRACT No. 4000127657/19/NL/FF/gp. The authors acknowledge support from the project JPI Climate Oceans EUREC4A-OA and Progetto Dipartimenti di Eccellenza, funded by MIUR 2018–2022. F. Desbiolles is supported by ESA contract n. 4000127657/19/NL/FF/gp and by HPC-TRES grant number 2020-10. A. N. Meroni acknowledges support from TWIGA project (H2020 program, grant No.776691), and ESA (contract n. 4000133281/20/I/NB). M. E. Hamouda is supported by Cariplo Foundation, EXTRA project, and HPC-TRES grant number 2017-03.

References

Bretherton, C. S., Widmann, M., Dymnikov, V. P., Wallace, J. M., & Bladé, I. (1999). The effective number of spatial degrees of freedom of a time-varying field. *Journal of Climate*, 12(7), 1990–2009. [https://doi.org/10.1175/1520-0442\(1999\)012<1990:tenosd>2.0.co;2](https://doi.org/10.1175/1520-0442(1999)012<1990:tenosd>2.0.co;2)

Businger, J., & Shaw, W. (1984). The response of the marine boundary layer to mesoscale variations in sea-surface temperature. *Dynamics of Atmospheres and Oceans*, 8(3–4), 267–281. [https://doi.org/10.1016/0377-0265\(84\)90012-5](https://doi.org/10.1016/0377-0265(84)90012-5)

Buzzi, A., Di Muzio, E., & Malguzzi, P. (2020). Barrier winds in the Italian region and effects of moist processes. *Bulletin of Atmospheric Science and Technology*, 1, 59–90.

Cassola, F., Ferrari, F., Mazzino, A., & Miglietta, M. M. (2016). The role of the sea on the flash floods events over Liguria (northwestern Italy). *Geophysical Research Letters*, 43, 3534–3542. <https://doi.org/10.1002/2016GL068265>

Chelton, D. B., Esbensen, S. K., Schlax, M. G., Thum, N., Freilich, M. H., Wentz, F. J., et al. (2001). Observations of coupling between surface wind stress and sea surface temperature in the eastern tropical Pacific. *Journal of Climate*, 14(7), 1479–1498. [https://doi.org/10.1175/1520-0442\(2001\)014<1479:ooocsw>2.0.co;2](https://doi.org/10.1175/1520-0442(2001)014<1479:ooocsw>2.0.co;2)

Chelton, D. B., Schlax, M. G., Freilich, M. H., & Milliff, R. F. (2004). Satellite measurements reveal persistent small-scale features in ocean winds. *Science*, 303(5660), 978–983. <https://doi.org/10.1126/science.1091901>

Chelton, D. B., Schlax, M. G., & Samelson, R. M. (2007). Summertime coupling between sea surface temperature and wind stress in the California current system. *Journal of Physical Oceanography*, 37(3), 495–517. <https://doi.org/10.1175/jpo3025.1>

Desbiolles, F., Blamey, R., Illig, S., James, R., Barimalala, R., Renault, L., & Reason, C. (2018). Upscaling impact of wind/sea surface temperature mesoscale interactions on southern Africa austral summer climate. *International Journal of Climatology*, 38(12), 4651–4660. <https://doi.org/10.1002/joc.5726>

Desbiolles, F., Blanke, B., Bentamy, A., & Grima, N. (2014). Origin of fine-scale wind stress curl structures in the Benguela and Canary upwelling systems. *Journal of Geophysical Research: Oceans*, 119(11), 7931–7948. <https://doi.org/10.1002/2014jc010015>

Desbiolles, F., Howard, E., Blamey, R. C., Barimalala, R., Hart, N. C., & Reason, C. J. (2020). Role of ocean mesoscale structures in shaping the Angola-Low pressure system and the southern Africa rainfall. *Climate Dynamics*, 54, 3685–3704.

Drobinski, P., Bastin, S., Arsouze, T., Béranger, K., Flaounas, E., & Stéfanon, M. (2018). North-western Mediterranean Sea-breeze circulation in a regional climate system model. *Climate Dynamics*, 51(3), 1077–1093. <https://doi.org/10.1007/s00382-017-3595-z>

- Ducrocq, V., Nuissier, O., Ricard, D., Lebeaupin, C., & Thouvenin, T. (2008). A numerical study of three catastrophic precipitating events over southern France. II: Mesoscale triggering and stationarity factors. *Quarterly Journal of the Royal Meteorological Society*, *134*, 131–145. <https://doi.org/10.1002/qj.199>
- Fiori, E., Comellas, A., Molini, L., Rebora, N., Siccardi, F., Gochis, D. J., et al. (2014). Analysis and hindcast simulations of an extreme rainfall event in the Mediterranean area: The Genoa 2011 case. *Atmospheric Research*, *138*, 13–29. <https://doi.org/10.1016/j.atmosres.2013.10.007>
- Fiori, E., Ferraris, L., Molini, L., Siccardi, F., Kranzmueller, D., & Parodi, A. (2017). Triggering and evolution of a deep convective system in the Mediterranean Sea: Modelling and observations at a very fine scale. *Quarterly Journal of the Royal Meteorological Society*, *143*, 927–941. <https://doi.org/10.1002/qj.2977>
- Foussard, A., Lapeyre, G., & Plougonven, R. (2019). Response of surface wind divergence to mesoscale SST anomalies under different wind conditions. *Journal of the Atmospheric Sciences*, *76*(7), 2065–2082. <https://doi.org/10.1175/jas-d-18-0204.1>
- Frenger, I., Gruber, N., Knutti, R., & Münnich, M. (2013). Imprint of Southern Ocean eddies on winds, clouds and rainfall. *Nature Geoscience*, *6*(8), 608–612. <https://doi.org/10.1038/ngeo1863>
- Gill, A. E. (2016). *Atmosphere—ocean dynamics*. Elsevier.
- Hayes, S. P., McPhaden, M. J., & Wallace, J. M. (1989). The influence of sea-surface temperature on surface wind in the eastern equatorial Pacific: Weekly to monthly variability. *Journal of Climate*, *2*(12), 1500–1506. [https://doi.org/10.1175/1520-0442\(1989\)002<1500:tiosst>2.0.co;2](https://doi.org/10.1175/1520-0442(1989)002<1500:tiosst>2.0.co;2)
- Hersbach, H., Bell, B., Berrisford, P., Hirahara, S., Horányi, A., Muñoz-Sabater, J., et al. (2020). The ERA5 global reanalysis. *Quarterly Journal of the Royal Meteorological Society*, *146*, 1999–2049.
- Kilpatrick, T., Schneider, N., & Qiu, B. (2014). Boundary layer convergence induced by strong winds across a midlatitude SST front. *Journal of Climate*, *27*(4), 1698–1718. <https://doi.org/10.1175/jcli-d-13-00101.1>
- Lebeaupin, C., Ducrocq, V., & Giordani, H. (2006). Sensitivity of torrential rain events to the sea surface temperature based on high-resolution numerical forecasts. *Journal of Geophysical Research*, *111*(D12), D12110. <https://doi.org/10.1029/2005jd006541>
- Li, Y., & Carbone, R. E. (2012). Excitation of rainfall over the tropical western Pacific. *Journal of the Atmospheric Sciences*, *69*(10), 2983–2994. <https://doi.org/10.1175/jas-d-11-0245.1>
- Lindzen, R. S., & Nigam, S. (1987). On the role of sea surface temperature gradients in forcing low-level winds and convergence in the tropics. *Journal of the Atmospheric Sciences*, *44*(17), 2418–2436. [https://doi.org/10.1175/1520-0469\(1987\)044<2418:otross>2.0.co;2](https://doi.org/10.1175/1520-0469(1987)044<2418:otross>2.0.co;2)
- Liu, X., Chang, P., Kurian, J., Saravanan, R., & Lin, X. (2018). Satellite-observed precipitation response to ocean mesoscale eddies. *Journal of Climate*, *31*, 6879–6895. <https://doi.org/10.1175/JCLI-D-17-0668.1>
- Ma, Z., Fei, J., Lin, Y., & Huang, X. (2020). Modulation of clouds and rainfall by tropical cyclone's cold wakes. *Geophysical Research Letters*, *47*, e2020GL088873. <https://doi.org/10.1029/2020GL088873>
- Madec, L. W., Chelton, D. B., & Esbensen, S. K. (2003). Observations of SST-induced perturbations of the wind stress field over the Southern Ocean on seasonal timescales. *Journal of Climate*, *16*(14), 2340–2354.
- Meroni, A. N., Giurato, M., Ragone, F., & Pasquero, C. (2020). Observational evidence of the preferential occurrence of wind convergence over sea surface temperature fronts in the Mediterranean. *Quarterly Journal of the Royal Meteorological Society*, *146*(728), 1443–1458. <https://doi.org/10.1002/qj.3745>
- Meroni, A. N., Parodi, A., & Pasquero, C. (2018). Role of SST patterns on surface wind modulation of a heavy midlatitude precipitation event. *Journal of Geophysical Research: Atmospheres*, *123*(17), 9081–9096. <https://doi.org/10.1029/2018jd028276>
- Meroni, A. N., Renault, L., Parodi, A., & Pasquero, C. (2018). Role of the oceanic vertical thermal structure in the modulation of heavy precipitations over the Ligurian Sea. *Pure and Applied Geophysics*, *175*(11), 4111–4130. <https://doi.org/10.1007/s00024-018-2002-y>
- Minobe, S., Kuwano-Yoshida, A., Komori, N., Xie, S.-P., & Small, R. J. (2008). Influence of the Gulf Stream on the troposphere. *Nature*, *452*(7184), 206–209. <https://doi.org/10.1038/nature06690>
- Nuissier, O., Ducrocq, V., Ricard, D., Lebeaupin, C., & Anquetin, S. (2008). A numerical study of three catastrophic precipitating events over southern France. I: Numerical framework and synoptic ingredients. *Quarterly Journal of the Royal Meteorological Society*, *134*(630), 111–130. <https://doi.org/10.1002/qj.200>
- Oerder, V., Colas, F., Echevin, V., Masson, S., Hourdin, C., Jullien, S., et al. (2016). Mesoscale SST-wind stress coupling in the Peru-Chile current system: Which mechanisms drive its seasonal variability? *Climate Dynamics*, *47*(7), 2309–2330. <https://doi.org/10.1007/s00382-015-2965-7>
- O'Neill, L. W., Chelton, D. B., & Esbensen, S. K. (2012). Covariability of surface wind and stress responses to sea surface temperature fronts. *Journal of Climate*, *25*(17), 5916–5942.
- O'Neill, L. W., Chelton, D. B., Esbensen, S. K., & Wentz, F. J. (2005). High-resolution satellite measurements of the atmospheric boundary layer response to SST variations along the Agulhas Return Current. *Journal of Climate*, *18*(14), 2706–2723.
- Park, K.-A., Cornillon, P., & Codiga, D. L. (2006). Modification of surface winds near ocean fronts: Effects of Gulf Stream rings on scatterometer (QuikSCAT, NSCAT) wind observations. *Journal of Geophysical Research*, *111*(C3), C03021. <https://doi.org/10.1029/2005jc003016>
- Pasquero, C., Desbiolles, F., & Meroni, A. N. (2021). Air-sea interactions in the cold wakes of tropical cyclones. *Geophysical Research Letters*, *48*, e2020GL091185. <https://doi.org/10.1029/2020GL091185>
- Pastor, F., Estrela, M. J., Peñarocha, D., & Millán, M. M. (2001). Torrential rains on the Spanish Mediterranean coast: Modeling the effects of the sea surface temperature. *Journal of Applied Meteorology*, *40*(7), 1180–1195. [https://doi.org/10.1175/1520-0450\(2001\)040<1180:trotsm>2.0.co;2](https://doi.org/10.1175/1520-0450(2001)040<1180:trotsm>2.0.co;2)
- Perlin, N., Kamenkovich, I., Gao, Y., & Kirtman, B. P. (2020). A study of mesoscale air-sea interaction in the Southern Ocean with a regional coupled model. *Ocean Modelling*, *153*, 101660. <https://doi.org/10.1016/j.ocemod.2020.101660>
- Press, W. H., Teukolsky, S. A., Vetterling, W. T., & Flannery, B. P. (1992). *Numerical recipes in C. The art of scientific computing* (Second edition). Cambridge University Press.
- Renault, L., Masson, S., Oerder, V., Jullien, S., & Colas, F. (2019). Disentangling the mesoscale ocean-atmosphere interactions. *Journal of Geophysical Research: Oceans*, *124*(3), 2164–2178. <https://doi.org/10.1029/2018JC014628>
- Rouault, M., Verley, P., & Backeberg, B. (2016). Wind changes above warm Agulhas Current eddies. *Ocean Science*, *12*, 495–506. <https://doi.org/10.5194/os-12-495-2016>
- Senatore, A., Furnari, L., & Mendicino, G. (2020). Impact of high-resolution sea surface temperature representation on the forecast of small Mediterranean catchments' hydrological responses to heavy precipitation. *Hydrology and Earth System Sciences*, *24*, 269–291. <https://doi.org/10.5194/hess-24-269-2020>
- Small, R. J., DeSzoeke, S. P., Xie, S. P., O'Neill, L., Seo, H., Song, Q., et al. (2008). Air-sea interaction over ocean fronts and eddies. *Dynamics of Atmospheres and Oceans*, *45*(3), 274–319. <https://doi.org/10.1016/j.dynatmoce.2008.01.001>

- Spall, M. A. (2007). Midlatitude wind stress-sea surface temperature coupling in the vicinity of oceanic fronts. *Journal of Climate*, *20*(15), 3785–3801. <https://doi.org/10.1175/jcli4234.1>
- Strobach, E., Molod, A., Trayanov, A., Forget, G., Campin, J.-M., Hill, C., & Menemenlis, D. (2020). Three-to-six-day air-sea oscillation in models and observations. *Geophysical Research Letters*, *47*, e2019GL085837. <https://doi.org/10.1029/2019GL085837>
- Villas Bôas, A. B., Sato, O. T., Chaigneau, A., & Castelão, G. P. (2015). The signature of mesoscale eddies on the air-sea turbulent heat fluxes in the South Atlantic Ocean. *Geophysical Research Letters*, *42*, 1856–1862. <https://doi.org/10.1002/2015GL063105>
- Wallace, J. M., Mitchell, T. P., & Deser, C. (1989). The influence of sea-surface temperature on surface wind in the eastern equatorial pacific: Seasonal and interannual variability. *Journal of Climate*, *2*(12), 1492–1499. [https://doi.org/10.1175/1520-0442\(1989\)002<1492:tiosst>2.0.co;2](https://doi.org/10.1175/1520-0442(1989)002<1492:tiosst>2.0.co;2)
- Wang, Q., Zhang, S.-P., Xie, S.-P., Norris, J. R., Sun, J.-X., & Jiang, Y.-X. (2019). Observed variations of the atmospheric boundary layer and stratocumulus over a warm eddy in the Kuroshio Extension. *Monthly Weather Review*, *147*, 1581–1591. <https://doi.org/10.1175/MWR-D-18-0381.1>
- Xu, H., Xu, M., Xie, S.-P., & Wang, Y. (2011). Deep atmospheric response to the spring kuroshio over the East China Sea. *Journal of Climate*, *24*(18), 4959–4972. <https://doi.org/10.1175/jcli-d-10-05034.1>